Electronic Properties of Realistic Anatase TiO_2 Nanoparticles from G_0W_0 Calculations on a Gaussian and Plane Waves Based Scheme

Ángel Morales-García*, Rosendo Valero, Francesc Illas

Departament de Ciència de Materials i Química Física & Institut de Química Teòrica i Computacional (IQTCUB), Universitat de Barcelona. c/ Martí i Franquès 1-11, 08028 Barcelona, Spain

Abstract

The electronic properties of realistic $(TiO_2)_n$ nanoparticles (NPs) with cuboctahedral and bipyramidal morphologies are investigated within the many body perturbation theory (MBPT) G_0W_0 approximation using PBE and hybrid PBEx (12.5% Fock contribution) functionals as starting points. The use of a Gaussian and plane waves (GPW) scheme reduces the usual O^4 computational time required in this type of calculations close to O^3 and thus allows considering explicitly NPs with n up to 165. The analysis of the Kohn-Sham energy orbitals and quasiparticle (QP) energies shows that the optical energy gap (O_{gap}), the electronic energy gap (E_{gap}) and the exciton binding energy (ΔE_{ex}) values decrease with increasing TiO_2 NP size, in agreement with previous work. However, while bipyramidal NPs appear to reach the scalable regime already for n = 84, cuboctahedral NPs reach this regime only above n =151. Relevant correlations are found and reported that will allow one predicting these electronic properties at the G_0W_0 level in even much larger NPs where these calculations are unaffordable. The present work provides a feasible and practical way to approach the electronic properties of rather large TiO_2 NPs and thus constitutes a further step in the study of realistic nanoparticles of semiconducting oxides.

INTRODUCTION

Accurate and affordable computational methods are required to properly describe the electronic properties of semiconducting materials. The prediction of these properties usually relies on band structure calculations carried out at different levels of theory. Since the 1970s, density functional theory (DFT) has become the standard tool to describe the physical and chemical properties of extended solids and finite systems.[1,2] Unfortunately, the broadly used local density approximation (LDA) and Generalized Gradient Approximation (GGA) implementations of DFT fail to predict the electronic properties of semiconductor materials resulting in a systematic underestimation of the calculated energy gap with respect to experiment.[3-5] To solve this critical issue several, more or less computational expensive, alternatives have been proposed including the use of the on-site Hubbard correction (the so called $+U$ approach)[6-8] or the use of hybrid functionals including a part of non-local Fock exchange.[9-12] Both of these approaches exhibit a semiempirical flavor since U or the amount of Fock exchange need to be chosen, usually by comparing to experiment. Different approaches have been proposed, and efficiently implemented, in the past few years that are both physically well-grounded and accurate in terms of comparing to experiment.[13,14] In particular, we mention the recent implementations of the many-body perturbation theory based *GW* formalism proposed by Hedin more than 50 years ago.[15-17] *GW* based techniques constitutes actually the state-of-the-art due to a good performance in predicting the energy gap in molecules and nanoparticles and also the band gap of bulk solids.[18-22] However, the high accuracy of the *GW* methods is accompanied by a very unfavorable scaling with respect to the size of the system that makes it difficult to approach the size of realistic systems composed by hundreds/thousands of atoms. For the first-order perturbative approximation of the *GW* method, usually referred to as G_0W_0, the scaling with size is as high as $O(N^4)$.[23-25]

The $O(N^4)$ dependence constitutes a real bottleneck when attempting to use these methods to approach the electronic properties of realistic systems such as semiconducting nanoparticles (NPs). These limitations have driven to reformulate the *GW* method for large scale calculations eliminating numerical approximations in the calculation of polarization, using efficient contour deformation techniques and providing a parallel implementation of the algorithm based on the splitting of both the single particle Green function and the screened Coulomb interaction.[26-28] Recently, an efficient algorithm to compute quasiparticle (QP) energies in the G_0W_0 formalism has displayed a reduction of the scaling of one order of magnitude to $O(N^3)$, thus allowing to tackle more realistic systems.[29] This novel formulation based on a Gaussian and plane waves (GPW) scheme with Resolution of the Identity (RI)[30] is selected herein to investigate the electronic properties of realistic titanium dioxide $(TiO_2)_n$ (n = 29–165) NPs composed of up to 495 atoms including cuboctahedral (or truncated bipyramidal) and octahedral (or bipyramidal) shapes as displayed in Figure 1 and described in more detail in a subsequent section. The results in the present work evidences that the scalable regime of these NPs is morphology dependent and unveils interesting correlations between Kohn-Sham orbital and G_0W_0 quasiparticle energies.

NANOPARTICLE MODELS AND COMPUTATIONAL STRATEGY

TiO_2 NPs have been widely studied from theoretical and experimental points of view due to their applications related to various technologies, including catalysis[31-33] and photocatalysis.[34-36] In particular, photocatalytic activity is related to the electronic structure based properties of the TiO_2 NPs[37,38] since these vary with size, shape and morphology as shown for models of realistic nanoparticles.[39] Clearly, high-level computational methods are required to provide accurate results and, hence, come out with reliable predictions. A rather recent work investigated the performance of the G_0W_0 method for the prediction of the electronic energy gap of small to medium size $(TiO_2)_n$ (n = 1–20) NPs,[40] as defined below, with structures obtained by a global optimization algorithm.[41] In spite of interesting trends, the TiO_2 NPs considered in previous work, containing up to 60 atoms are too small to provide information about realistic systems and hence, analysis of larger TiO_2 NPs is required to better link theoretical predictions with the experiment. Here, we focus on the electronic properties considering optical (O_{gap}), electronic (E_{gap}) energy gaps, and exciton binding energy (ΔE_{ex}) of realistic titanium dioxide $(TiO_2)_n$ NPs with n = 29–165. As in previous works,[39,40] O_{gap} is estimated from the difference between the highest occupied molecular orbital (HOMO) and the lowest unoccupied molecular orbital (LUMO) defined from the Kohn-Sham orbital energies. This is a reasonably good approximation as shown in a recent study comparing the thus defined O_{gap} to results arising from frequency-dependent dielectric function;[42] and is in agreement with the interpretation proposed by Baerends *et al*.[43] On the other hand, E_{gap} is calculated from differences in the QP energies (G_0W_0) for HOMO and LUMO (QP_{HOMO} and QP_{LUMO}) and thus corresponds to the difference between vertical ionization potential and electron affinity. Finally, ΔE_{ex} is estimated as the difference between E_{gap} and O_{gap} and provides information related to the electron–hole pair interaction energy. Note that, in absence of optical excitons, ΔE_{ex} vanishes when the system size becomes sufficiently large.

All calculations presented here have been carried out by using a GPW scheme for solving Kohn-Sham equations as implemented in the CP2K code.[44,45] The hybrid scheme employs a Gaussian basis to expand molecular orbitals and an auxiliary plane-wave basis for the expansion of the electronic density. In order to have an efficient expansion of the density in plane waves, core electrons are replaced by pseudopotentials. Dual-space norm-conserving and relativistic pseudopotentials of the Goedecker-Teter-Hutter (GTH) type[46] parametrized for PBE[47] have been selected for oxygen (O) and titanium (Ti) atoms.[48] Importantly, we have adopted a recently implemented algorithm which for G_0W_0 calculations has a computational cost scaling close to $O(N^3)$.[49] This makes it possible to tackle significantly larger systems than with the standard algorithm exhibiting a $O(N^4)$ scaling.

In principle, *GW* calculations can be carried out in a self-consistent way and in that case final results do not depend on the initial density used to build the Green's function and screening potential.[50] However, those calculations are excessively demanding, even for simple systems containing a few atoms only. In practice, one relies on the G_0W_0 approach which leads to reasonable results[51] although these do depend on the initial starting density.[52] To investigate the effect of the initial density, the present G_0W_0 calculations are

carried out starting from the PBE density (G_0W_0@PBE) and also from that obtained from the PBEx hybrid functional including a 12.5% of non-local Fock exchange (G_0W_0@PBEx) which has proven to appropriately describe stoichiometric and reduced bulk anatase and rutile.[39] To carry out the G_0W_0@PBEx calculations, auxiliary density matrix method (ADMM) basis sets are used in order to deal with the hybrid part of the functional.[53] The ADMM basis sets have only been employed for the double-zeta primary basis sets, because they make the convergence of Hartree-Fock exchange (HFX) difficult with the standard HFX approach. For the primary Gaussian basis sets, we employ valence-only basis sets of double-zeta (DZ) and triplet-zeta (TZ) quality. The double-zeta basis sets are labeled as DZVP-MOLOPT-GTH for O atom and DZVP-MOLOPT-SR-GTH for Ti atom,[54] and triple-zeta basis sets are denoted cc-TZ for both oxygen and titanium.[55] In addition, the solution of the *GW* equations adopted here is made through the RI approximation.[56] For both primary basis sets, an auxiliary basis set denoted RI_TZ has been used for oxygen, and both the cc-TZ basis set and another basis set denoted RI have been used as auxiliary bases for titanium. The coefficients of the primary, RI, and ADMM basis sets, along with a sample CP2K input file, are presented in Supporting Information (SI).

RESULTS AND DISCUSSION

We start this section discussing the influence that primary basis set (see Tables S1 and S2 in SI) has on the O_{gap} and E_{gap} of TiO_2 NPs by using the mean absolute error (MAE) incurred by using the smaller DZ basis set with respect to the larger cc-TZ one. The MAE descriptor indicates 0.05 (0.07) and 0.19 (0.21) eV for O_{gap} and E_{gap}, respectively, corresponding to the PBE and the hybrid PBEx exchange correlation functionals with the latter one in brackets. Note that there are no significant deviations in either energy gap (±0.02 eV) between PBE and PBEx. However, MAE is larger for E_{gap} than for O_{gap} showing that the size of the primary basis set has a larger effect on QP energies regardless of the functional employed. Following previous convergence tests[57] and given the large dimensions of TiO_2 NPs studied here, we assume that primary TZ basis set shows the best performance to describe properly the electronic properties of TiO_2 NPs. Primary DZ basis overestimates E_{gap} leading consequently, to overestimation of ΔE_{ex} compared with those values predicted with TZ basis (see Tables S1 and S2 for further details).

Once the effect of primary basis set is assessed, we tackle the analysis of the trend in the HOMO and LUMO orbital energies, and the subsequent O_{gap} with increasing NP size by using the Kohn-Sham (KS) orbital energies obtained by PBE and hybrid PBEx functionals. Later, an analogous discussion will be presented considering QP energies associated to HOMO and LUMO orbitals, and the subsequent E_{gap} derived from G_0W_0@PBE and G_0W_0@PBEx based calculations. The former analysis depicted in Figure S1 shows two clear decreasing trends for both HOMO and LUMO KS orbital energies with TiO_2 NP size regardless of the employed functional. The large values of the smallest sized TiO_2 NPs correspond to the pronounced quantum confinement effect, which vanishes smoothly by increasing the TiO_2 NP size.[58,59] An interesting result is the marked effect of the NP morphology. In general, TiO_2 NPs with cuboctahedral morphology feature systematically larger HOMO and LUMO orbital energies (in absolute values) than NPs with bipyramidal

morphology (see Figure S1). We attribute this systematic trend to the exposed surfaces; bypiramidal TiO_2 NPs exhibit six (101) facets, whereas, cuboctahedral NPs expose simultaneously (101) and (001) facets. Similar tendencies are observed for values arising from calculations with the hybrid PBEx functional (see Figure S1, bottom panels). However, note that the PBEx functional promotes an opening of the energy gap by inducing downshifts and upshifts in HOMO and LUMO orbital energies, respectively.[60] In this way, the resulting O_{gap} shows a clear reduction of its value with increasing TiO_2 NP size, in agreement with previous results.[61] Note, however, that the differences observed in the HOMO and LUMO orbital energies induced by the different morphology cancel out and, hence, a unique trend encompasses both families of TiO_2 NPs. Only in the case of the $(TiO_2)_{97}$ NP the orbital energies are partially downshifted relative to this general trend, an effect due to its particular structure directly related with exposed (101) and (001) surfaces ratio. This is the only nanoparticle where the ratio between exposed surfaces is favorable for (001) and hence its O_{gap} has a lower value, as expected.[61]

By using the first-order perturbation G_0W_0 approach, the ionization energies and electron affinities are calculated from QP_{HOMO} and QP_{LUMO} energies, respectively (see Figure 2). As mentioned earlier, these calculations demand the use of the larger auxiliary RI basis set raising significantly the computational cost of *GW* calculations. The effect of going from the auxiliary cc-TZ to the RI basis set (for Ti atoms) is analyzed in detail on the smallest $(TiO_2)_n$ (n=29 and 35) NPs comparing the QP energies and E_{gap} for cc-TZ as primary basis and with cc-TZ or RI as auxiliary basis sets by using PBE and hybrid PBEx functionals (see Tables S3 and S4). Note that each selected TiO_2 NP is a representative case for each one of the TiO_2 morphologies investigated here (see Figure 1). These calculations show that the change of auxiliary basis set from cc-TZ to RI promotes systematic downshifts and upshifts on QP_{HOMO} and QP_{LUMO}, respectively. Focusing on G_0W_0@PBEx results, QP_{HOMO} and QP_{LUMO} shift -0.23 and 0.24 eV in absolute values for $(TiO_2)_{29}$, and -0.23 and 0.22 eV for $(TiO_2)_{35}$. Consequently, with the RI basis, E_{gap} increases its value by 0.46 and 0.44 eV for $(TiO_2)_{29}$ and $(TiO_2)_{35}$ NPs set relative to the same values calculated with cc-TZ as auxiliary basis set (Table S4); a similar behavior is observed for calculations performed with PBE functional (Table S3). The choice of the RI auxiliary basis set instead of the cc-TZ in the CP2K calculations is justified by the very good match between E_{gap} values from the present G_0W_0 calculations for these two TiO_2 NPs to those obtained by using a relativistic all-electron description with numerical atomic-centered orbital basis set as implemented in FHI-aims code[62] (Tables S3 and S4. See Ref. 40 for further computational details). The energy shifts (Tables S3 and S4) induced on QP_{HOMO} and QP_{LUMO} when going from cc-TZ to RI auxiliary basis set are assumed to be consistently the same for the larger TiO_2 NPs and the final results are shown in Figure 2. Note that resemblances between the trends of QP_{HOMO}-QP_{LUMO} (Figure 2) and HOMO-LUMO energies (Figure S1) are found, showing again the mentioned morphology-induced distinction. The cuboctahedral NPs show lower ionization energies and electron affinities in absolute values than the bipyramidal ones. This systematic agreement between both analyses depicted in Figures S1 and 2 is not surprising because QP energies depend noticeably on the starting point, that is, on the "arbitrary" set of Kohn-Sham eigenvalues and orbitals

calculated by either PBE or PBEx functionals. The resulting E_{gap} values follow the expected trend reducing its value with the number of TiO_2 units (Figure 2). This result is fully consistent with a previous study where E_{gap} is estimated by using ΔSCF approach based on all electron relativistic DFT including numerical atom-centered orbitals.[40]

Next, we analyze the exciton binding energy (ΔE_{ex}) that provides the strength of electron-hole interaction. The trend on the calculated ΔE_{ex} provides a direct measure of the convergence of electronic properties toward the bulk where it vanishes due to the low exciton binding energy in bulk TiO_2. This behavior is clearly shown in Figure 3 for both PBE and PBEx calculations and is in line with previous results based on ΔSCF calculations.[61] Looking at PBEx results, ΔE_{ex} exhibits a decreasing trend with the number of TiO_2 units from 2.6 to 2.1 eV. The bipyramidal TiO_2 NPs (red squares in Figure 3) have an exciton binding energy difference of 0.09 eV corresponding to the difference between $(TiO_2)_{84}$ and $(TiO_2)_{165}$. This result is an indication that, at this size, TiO_2 NPs with bipyramidal shape are close to the scalable regime limit. This is, where properties of NPs scale linearly towards bulk limit values. On the other hand, for the cuboctahedral TiO_2 NPs (blue squares in Figure 3) the ΔE_{ex} difference between $(TiO_2)_{78}$ and $(TiO_2)_{151}$ is as large as 0.16 eV. This result indicates that TiO_2 NPs with bipyramidal shape reach the scalable regime limit at lower sizes than truncated octahedral NPs. Note also that in the case of the cuboctahedral $(TiO_2)_{97}$ NP, ΔE_{ex} is far away from the general trend observed (see Figure 3), a clear consequence of the exposed (001) facets. In spite of that, for a given NP size, themagnitude of ΔE_{ex} distinguishes TiO_2 NPs with different morphology, a new and important observation, following the tendencies towards the scalable regime limit.

Finally, interesting systematic correlations are found between E_{gap} and O_{gap}. The amount of Fock exchange in the functional has a pronounced effect mainly on O_{gap}, as recently reported[60] and in agreement with the well-established general trend that hybrid functionals lead to improved predictions of band gap in oxides and similar systems.[63,64] Consequently, the calculated E_{gap} values also depend on such effect, since the KS orbital energies are the starting point to calculate E_{gap} *via* G_0W_0 approach. This is the main reason why two different linear fits are observed in Figure 4a. An analogous tendency was obtained with TiO_2 NPs below 20 units.[40] However, the correlations emerging from the present work considerable improve those based on smaller NPs.

Focusing on the performance of the MBPT based G_0W_0 method, we observe that the Fock contribution effect on the calculated E_{gap} is quite lower than on O_{gap}. This comes from the relatively small deviation of the correlation found between $E_{gap}(G_0W_0@PBEx)$ and $E_{gap}(G_0W_0@PBE)$ with respect to the ideal correlation as depicted in Figure 4b. We conclude that both correlations may be useful to predict the electronic properties of TiO_2 NPs composed by thousands of atoms with a G_0W_0 precision by relying on standard DFT calculations. In particular, the present results show that it is possible to obtain values of E_{gap} of G_0W_0@PBEx quality from E_{gap} computed at G_0W_0@PBE level, which in turn can be obtained from PBE KS orbital energies through O_{gap} and the correlation in Figure 4a.

CONCLUSIONS

In this work, a Gaussian and plane wave scheme has been used to approach the electronic properties of $(TiO_2)_n$ (n = 29–165) NPs composed by up to 495 atoms at the G_0W_0 level of theory considering either PBE or hybrid PBEx functionals as starting points. These calculations are possible thanks to the reduction in the usual O^4 computational time to close to O^3.

The cuboctahedral and bipyramidal NP morphologies exhibit different trends in the Kohn-Sham orbital and QP energies suggesting that this provides an electronic structure descriptor to discriminate them from photoemission experiments. In agreement with previous work,[61] O_{gap} and E_{gap} decrease with the NP size regardless of the exchange correlation functional employed. The introduction of non-local Fock exchange in the functional induces a gap opening when going from PBE to PBEx, consequently $E_{gap}(G_0W_0)$ undergoes a similar gap opening giving larger $E_{gap}(G_0W_0$@PBEx) value larger than $E_{gap}(G_0W_0$@PBE). Also, a larger contribution of Fock exchange is observed in the calculation of O_{gap}, as expected from previous works.[63,64] The observed shift between PBE and PBEx functionals is also reflected on the caclulated ΔE_{ex} values.

From the more reliable PBEx results, it turns out that the bipyramidal TiO_2 NPs reach the scalable regime at smaller sizes with ΔE_{ex} trending to bulk faster than for the NPs with cuboctahedral morphology. Moreover, the correlation obtained between E_{gap} and O_{gap} will be useful to predict the former quantity, at either G_0W_0@PBE or G_0W_0@PBEx level, for large TiO_2 NPs just from the KS orbital energies through O_{gap} rather than from the QPs which would require large computational resources.

Finally, one must point out that the differences in the QPs predicted from G_0W_0@PBE and G_0W_0@PBEx indicate that calculated results are not fully converged within the G_0W_0 formalism. Nevertheless, it is expected that results arising from the use of a hybrid functional as starting point are closer to the experiment as inferred from such comparison in some systems.[65,66]

ASSOCIATED CONTENT

The Supporting Information is available free of charge on the ACS Publications website at DOI:

Tables S1 and S2 list the electronic properties of TiO_2 NPs for DZ and TZ basis set with PBE and hybrid PBEx functionals, respectively. Figure S1 correspond to the evolution of HOMO and LUMO orbital KS energies with TiO_2 NP size. Tables S3 and S4 compiles the comparison between CP2K and FHI-AIMS codes. Finally, the CP2K basis sets employed are described by using the CP2K inputs.

AUTHOR INFORMATION

Corresponding Author

*E-mail: angel.morales@ub.edu

Notes

The authors declare no competing financial interest.

ACKNOWLEDGMENTS

The research reported in this work has been supported by the Spanish MINECO/FEDER CTQ2015-64618-R, MICIUN RTI2018-095460-B-I00 and *María de Maeztu* MDM-2017-0767 grant and, in part, by Generalitat de Catalunya 2017SGR13 and XRQTC grants. A. M.-G. thanks to Spanish MICIUN for the *Juan de la Cierva* postdoctoral grant (IJCI-2017-31979) and F. I. acknowledges additional support from the 2015 ICREA Academia Award for Excellence in University Research. Computational time at the MareNostrum Supercomputer has been provided by the Barcelona Supercomputing Centre (BSC) through the Partnership for Advanced Computing in Europe (PRACE) EXCIPHOCAT project (2016163940).

Figure 1. Scheme of $(TiO_2)_n$ (n = 29–165) nanoparticles, which are obtained by using top-down approach. Anatase-type truncated octahedral (cuboctahedron) and anatase-type octahedral (bipyramid) shapes are distinguished by orange and green labels, respectively. Red and blue spheres stand for to O and Ti atoms, respectively. Note that bipyramid TiO_2 NPs feature only the (101) surface and the cuboctahedron TiO_2 ones exhibit both (101) and (001) surfaces. Further details about the atomic structure can be found in ref. 61.

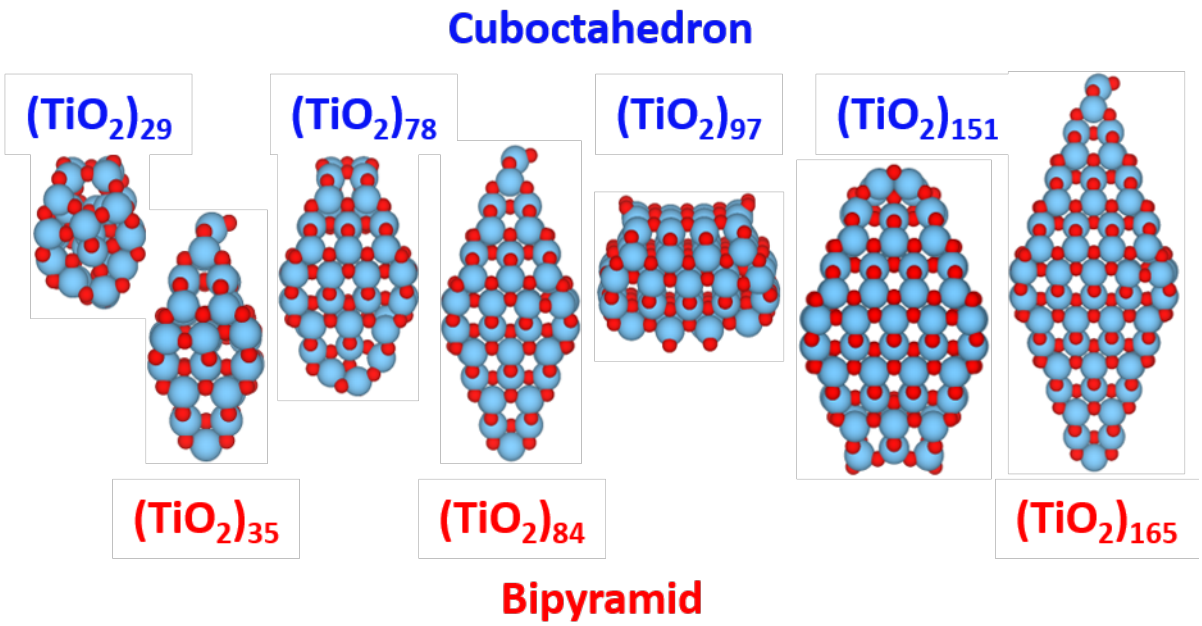

Figure 2. Trends of quasiparticle (QP) energies of HOMO and LUMO energy orbitals, and E_{gap} with TiO_2 NP size. Upper panels correspond to G_0W_0@PBE calculations and the bottom ones show the results of G_0W_0@PBEx calculations. Cuboctahedron and bipyramid shapes are clearly distinguished by blue and red colors, respectively.

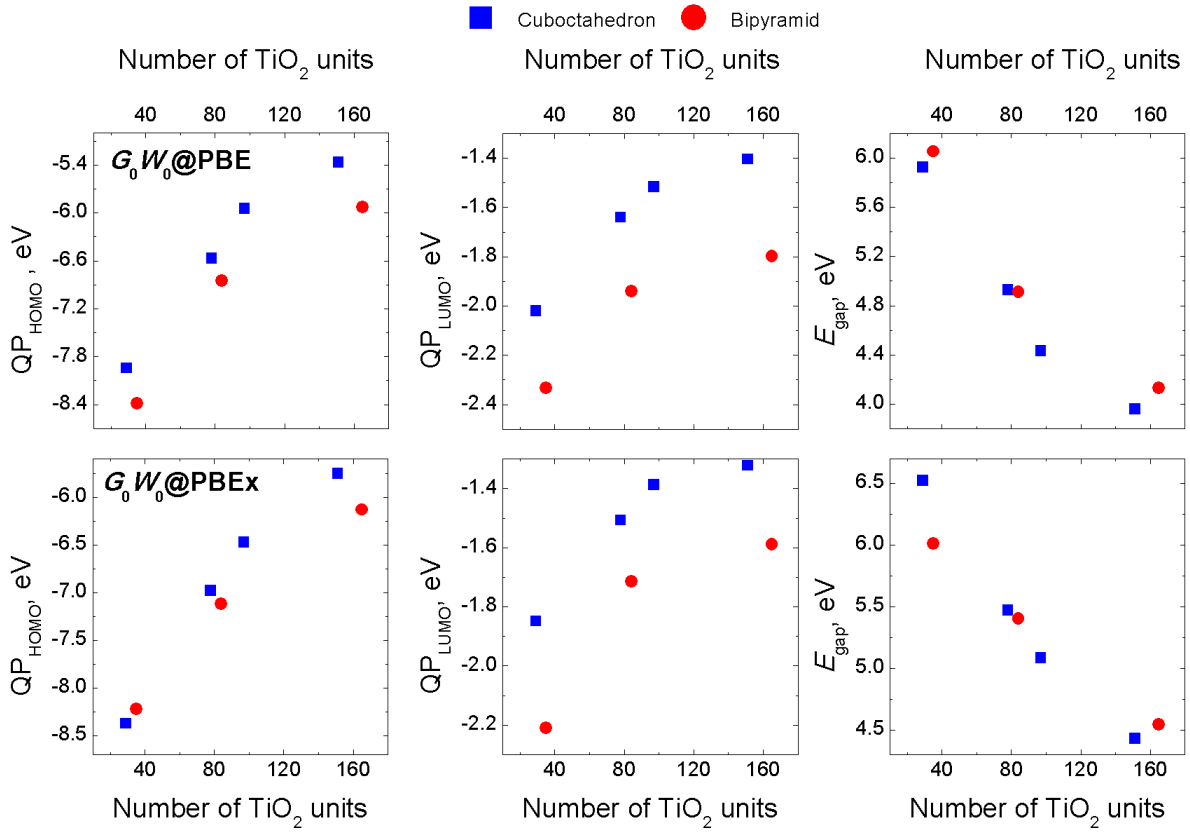

Figure 3. Exciton binding energy of $(TiO_2)_n$ NPs with cuboctahedral (blue circles and squares) and bipyramidal (red circles and squares) shapes. Note that circles and squares correspond to PBE and PBEx calculations, respectively. Green and gray regions are included to distinguish the tendencies obtained with PBE and hybrid PBEx functionals, respectively.

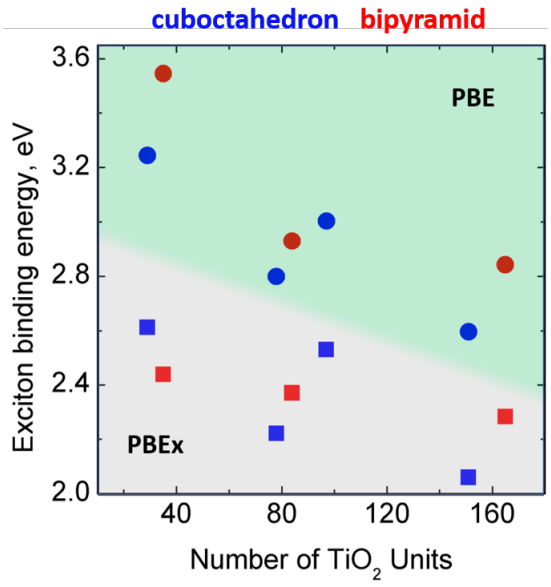

Figure 4. Linear correlations between (a) E_{gap} and O_{gap} for PBE and PBEx calculations, and (b) $E_{gap}(G_0W_0@PBEx)$ *versus* $E_{gap}(G_0W_0@PBE)$. Fitting equations are reported in the inset of figures. In Figure 4a circles and squares denote the PBE and PBEx calculations, respectively. In Figure 4b red circles and blue squares describe bypiramidal and cuboctahedron TiO_2 NPs, respectively.

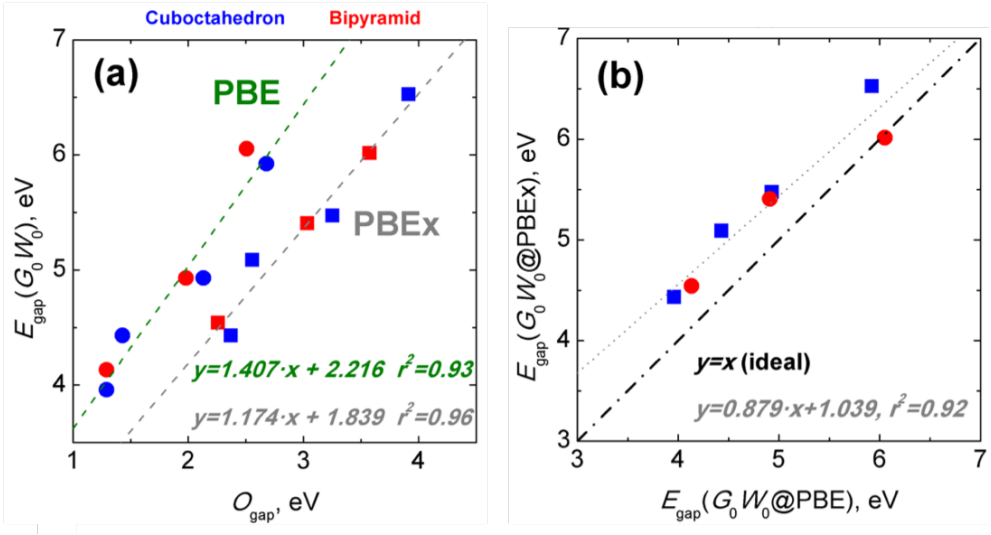

REFERENCES

(1) Hohenberg, P.; Kohn, W. Inhomogeneous Electron Gas. *Phys. Rev.* **1964**, *136*, B864-B871.

(2) Kohn, W.; Sham, L. J. Self-Consistent Equations Including Exchange and Correlation Effects. *Phys. Rev.* **1965**, *140*, A1133-A1138.

(3) Perdew, J. P. Density Functional Theory and the Band Gap Problem. *Int. Quantum Chem.* **1985**, *28*, 497-523.

(4) Sousa, C.; Tosoni, S.; Illas, F. Theoretical Approaches to Excited-State-Related Phenomena in Oxide Surfaces. *Chem. Rev.* **2013**, *113*, 4456-4495.

(5) Seidl, A.; Görling, A.; Vogl, P.; Majewski, J. A.; Levy, M. Generalized Kohn-Sham Schemes and the Band-Gap Problem. *Phys. Rev. B: Condens. Matter Mater. Phys.* **1996**, *53*, 3764-3774.

(6) Anisimov, V. I.; Zaanen, J.; Andersen, O. K. Band Theory and Mott Insulators: Hubbard U Instead of Stoner I. *Phys. Rev. B: Condens. Matter Mater. Phys.* **1991**, *44*, 943-954.

(7) Dudarev, S. L.; Botton, G. A.; Savroasov, S. Y.; Humphreys, C. J.; Sutton, A. P. Electron-Energy Loss Spectra and the Structural Stability of Nickel Oxide: An LSDA+U Study. *Phys. Rev. B: Condens. Matter Mater. Phys.* **1998**, *57*, 1505-1509.

(8) Mosey, N. J.; Carter, E. A. Ab Initio Evaluation of Coulomb and Exchange Parameters for DFT+U Calculations. *Phys. Rev. B: Condens. Matter Mater. Phys.* **2007**, *76*, 155123.

(9) Muscat, J.; Wander, A.; Harrison, N. M. On the Prediction of Band Gaps from Hybrid Functional Theory. *Chem. Phys. Lett.* **2001**, *342*, 397-401.

(10) Becke, A. D. A New Mixing of Hartree-Fock and Local Density-Functional Theories. *J. Chem. Phys.* **1993**, *98*, 1372.

(11) Xiao, H.; Tahr-Kheli, J.; Goddard III, W. A. Accurate Band Gaps for Semiconductors from Density Functional Theory. *J. Phys. Chem. Lett.* **2011**, *2*, 212-217.

(12) Garza, A. J.; Scuseria, G. E. Predicting Band Gaps with Hybrid Density Functionals. *J. Phys. Chem. Lett.* **2016**, *7*, 4165-4170.

(13) Johnson, K. A.; Ashcroft, N. W. Corrections to Density-Functional Theory Band Gaps. *Phys. Rev. B: Condens. Matter Mater. Phys.* **1998**, *58*, 15548-15556.

(14) Remediakis, I. N.; Kaxiras, E. Band-Structure Calculations for Semiconductors within Generalized-Density-Functional Theory. *Phys. Rev. B: Condens. Matter Mater. Phys.* **1999**, *59*, 5536-5543.

(15) Hedin, L. New method for calculating the one-particle Green's function with application to the electron-gas problem. *Phys. Rev.* **1965**, *139*, A796-A823.

(16) Aryasetiawan, F.; Gunnarsson, O. The *GW* method. *Rep. Prog. Phys.* **1998**, *61*, 237-312.

(17) Onida, G.; Reining, L.; Rubio, A. Electronic Excitations: Density-Functional versus Many-Body Green´s-Function Approaches. *Rev. Mod. Phys.* **2002**, *74*, 601-659.

(18) Caruso, F.; Dauth, M.; van Setten, M. J.; Rinke P. Benchmark of *GW* Approaches for the *GW*100 Test Set. *J. Chem. Theory Comput.* **2016**, *12*, 5076-5087.

(19) Kaplan, F.; Harding, M. E.; Seiler, C.; Weigend, F.; Evers, F.; van Setten, M. J. Quasi-Particle Self-Consistent *GW* for Molecules. *J. Chem. Theory Comput.* **2016**, *12*, 2528-2541.

(20) Van Setten, M. J.; Caruso, F.; Sharifzadeh, S.; Ren, X.; Scheffler, M.; Liu, F.; Lischner, J.; Lin, L.; Deslippe, J. R.; Louie, S. G.; Yang, C.; Weigend, F.; Neaton, J. B.; Evers, F.; Rinke P. *GW*100: Benchmarking G_0W_0 for Molecular Systems. *J. Chem. Theory Comput.* **2015**, *11*, 5665-5687.

(21) Ergönenc, Z.; Kim, B.; Liu, P.; Kresse, G.; Franchini, C. Converged *GW* Quasiparticle Energies for Transition Metal Oxide Perovskites. *Phys. Rev. Materials* **2018**, *2*, 024601 (1-16).

(22) Marom, N.; Accurate Description of the Electronic Structure of Organic Semiconductors by *GW* Methods. *J. Phys.: Condens. Matter* **2017**, *29*, 103003 (1-20).

(23) Friedrich C.; Blügel S.; Achindlmayr A. Efficient Implementation of the *GW* Approximation within the All-Electron FLAPW Method. *Phys. Rev. B* **2010**, *81*, 125102.

(24) Ren, X.; Rinke, P.; Blum, V.; Wieferink, J.; Tkatchenko, A.; Sanfilippo, A.; Reuter, K.; Scheffler, M. Resolution-of-Identity Approach to Hartree-Fock, Hybrid Density Functionals, RPA, MP2 and *GW* with Numeric Atom-Centered Orbital Basis Functions. *New J. Phys.* **2012**, *14*, 053020.

(25) Gao, W.; Xia, W.; Gao, X.; Zhang, P. Speeding up *GW* Calculations to Meet Challenge of Large Scale Quasiparticle Predictions. *Sci. Rep.* **2016**, *6*, 36849.

(26) Nguyen, H.-V.; Pham, T. A.; Rocca, D.; Galli, G. Improving Accuracy and Efficiency of Calculations of Photoemission Spectra within the Many-Body Perturbation Theory. *Phys. Rev. B* **2012**, *85*, 081101(R) (1-5)

(27) Pham, T. A.; Nguyen, H.-V.; Rocca, D.; Galli, G. *GW* Calculations Using the Spectral Decomposition of the Dielectric Matrix: Verification, Validation, and Comparison of Methods. *Phys. Rev. B* **2013**, *87*, 155148 (1-12).

(28) Govoni, M.; Galli, G. Large Scale *GW* Calculations. *J. Chem. Theory Comput.* **2015**, *11*, 2680-2696.

(29) Wilhelm, J.; Golze, D.; Talirz, L.; Hutter, J.; Pignedoli, C. A. Toward *GW* Calculations on Thousands of Atoms. *J. Phys. Chem. Lett.* **2018**, *9*, 306-312.

(30) Lippert, G.; Hutter, J.; Parrinello, M. A Hybrid Gaussian and Plane Wave density Functional Scheme. *Mol. Phys.* **1997**, *92*, 477-487.

(31) Bagheri, S.; Julkapli, N. M.; Hamid, S. B. A. Titanium Dioxide as a Catalyst Support in Heterogeneous Catalysis. *The Scientific World Journal* **2014**, *21*, 727496.

(32) Weiher, N.; Beesley, A. M.; Tsapatsaris, N.; Delannoy, L.; Louis, C.; van Bokhoven, J. A.; Schroeder, S. L. M. Activation of Oxygen by Metallic Gold in Au/TiO2 Catalysts. *J. Am. Chem. Soc.* **2007**, *129*, 2240-2241.

(33) Wang, Y.-G-: Cantu, D. C.; Lee, M.-S.; Li, J.; Glezakou, V.-A.; Rousseau, R. CO Oxidation on Au/TiO_2: Condition-Dependent Active Sites and Mechanistic Pathways. *J. Am. Chem. Soc.* **2016**, *138*, 10467-10476.

(34) Fujishima, A.; Honda, K. Electrochemical Photolysis of Water at a Semiconductor Electrode. *Nature* **1972**, *238*, 37-38.

(35) Schneider, J.; Matsuoka, M.; Takeuchi, M.; Zhang, J.; Horiuchi, Y.; Anpo, M.; Bahnemann, D. W. Understanding TiO2 Photocatalysis: Mechanism and Materials. *Chem. Rev.* **2014**, *114*, 9919-9986.

(36) Li, W.; Elzatahry, A.; Aldhayan, D.; Zhao, D. Core-Shell Structured Titanium Dioxide Nanomaterials for Solar Energy Utilization. *Chem. Soc. Rev.* **2018**, *47*, 8203-8237.

(37) Meng, Q.; Wang, T.; Liu, E.; Ma, X.; Ge, Q.; Gong, J. Understanding Electronic and Optical Properties of Anatase TiO_2 Photocatalysts co-Doped with Nitrogen and Transition Metals. *Phys. Chem. Chem. Phys.* **2013**, *15*, 9549-9561.

(38) Yates Jr, J. T. Photochemistry on TiO_2: Mechanisms behind the Surface Chemistry. *Surf. Sci.* **2009**, *603*, 1605-1612.

(39) Cho, D.; Ko, K. C.; Lamiel-García, O.; Bromley, S. T.; Lee, J. Y.; Illas, F. Effect of Size and Structure on the Ground-State and Excited-State Electronic Structure of TiO2 Nanoparticles. *J. Chem. Theory Comput.* **2016**, *12*, 3751-3763.

(40) Morales-García, Á.; Valero, R.; Illas, F. Performance of the G_0W_0 Method in Predicting the Electronic Gap of TiO_2 Nanoparticles. *J. Chem. Theory Comput.* **2017**, *13*, 3746-3753.

(41) Lamiel-García, O.; Cuko, A.; Calatayud, M.; Illas, F.; Bromley, S. T. Predicting Size-Dependent Emergence of Crystallinity in Nanomaterials: Titania Nanoclusters *versus* Nanocrystals. *Nanoscale* **2017**, *9*, 1049-1058.

(42) Valero, R.; Morales-García, Á.; Illas, F. Theoretical Modeling of Electronic Excitations of Gas-Phase and Solvated TiO_2 Nanoclusters and Nanoparticles of Interest in Photocatalysis. *J. Chem. Theory Comput.* **2018**, *14*, 4391-4404.

(43) Baerends, E. J.; From the Kohn-Sham Band Gap to the Fundamental Gap in Solids. An Integer Electron Approach. *Phys. Chem. Chem. Phys.* **2017**, *19*, 15639-15656.

(44) The CP2K developers' group, CP2K is freely available. **2016**. http://www.cp2k.org/.

(45) Hutter, J.; Ianuzzi, M.; Schiffmann, F.; VandeVondele, J. CP2K: Atomistic Simulations of Condensed Matter Systems. *WIREs Comput. Mol. Sci.* **2014**, *4*, 15-25.

(46) Goedecker, S.; Teter, M.; Hutter, J. Separable Dual-Space Gaussian Pseudopotentials. *Phys. Rev. B* **1996**, *54*, 1703-1710.

(47) Perdew, J. B.; Burke, K.; Ernzerhof, M. Generalized Gradient Approximation Made Simple. *Phys. Rev. Lett.* **1996**, *77*, 3865-3868.

(48) Krack, M. Pseudopotentials for H to Kr Optimized for Gradient-Corrected Exchange-Correlation Functionals. *Theor. Chem. Acc.* **2005**, *114*, 145-152.

(49) Wilhelm, J.; Golze, D.; Talirz, L.; Hutter, J.; Pignedoli, C. A. Toward GW Calculations with Thousands of Atoms. *J. Phys. Chem. Lett.* **2018**, *9*, 306-312.

(50) Koval, P.; Foerster, D.; Sánchez-Portal, D. Fully Self-Consistent *GW* and Quasiparticle Self-Consistent *GW* for Molecules. *Phys. Rev. B* **2014**, *89*, 155417.

(51) Marom, N. Accurate description of the Electronic Structure of Organic Semiconductors by *GW* Methods. *J. Phys.: Condens. Matter* **2017**, *29*, 103003.

(52) Körzdörfer, T.; Marom, N. Strategy for Finding a Reliable Starting Point for G_0W_0 Demonstrated for Molecules. *Phys. Rev. B* **2012**, *86*, 041110(R).

(53) Guidon, M.; Hutter, J.; VandeVondele, J. Auxiliary Density Matrix Methods for Hartree-Fock Exchange Calculations. *J. Chem. Theory Comput.* **2010**, *6*, 2348-2364.

(54) VandeVondele, J.; Hutter, J. Gaussian Basis Sets for Accurate Calculations on Molecular Systems in Gas and Condensed Phases. *J. Chem. Phys.* **2007**, *127*, 114105/1-9.

(55) Spreafico, C.; VandeVondelle, J. The Nature of Excess Electrons in Anatase and Rutile from Hybrid DFT and RPA. *Phys. Chem. Chem. Phys.* **2014**, *16*, 26144-16152.

(56) Del Ben, M.; Hutter, J.; VandeVondelle, J. Electron Correlation in the Condensed Phase from a Resolution of Identity Approach Based on the Gaussian and Plane Waves Scheme. *J. Chem. Theory Comput.* **2013**, *9*, 2654-2671.

(57) Wilhelm, J.; Del Ben, M.; Hutter, J. *GW* in the Gaussian and Plane Waves Scheme with Application to Linear Acenes. *J. Chem. Theory Comput.* **2016**, *12*, 3623-3635.

(58) Chen, X.; Mao, S. S. Titanium Dioxide Nanomaterials Synthesis, Properties, Modifications and Applications. *Chem. Rev.* **2007**, *107*, 2891-2959.

(59) Peng, H.; Li, J. Quantum Confinement and Electronic Properties of Rutile TiO2 Nanowires. *J. Phys. Chem. C* **2008**, *112*, 20241-20245.

(60) Morales-García, Á.; Valero, R.; Illas, F.; Reliable and Computationally Affrodable Prediction of the Energy Gap of $(TiO_2)_n$ ($10 \leq n \leq 563$) Nanoparticles from Density Functional Theory. *Phys. Chem. Chem. Phys.* **2018**, *20*, 18907-18911.

(61) Lamiel-García, O.; Ko, K. C.; Lee, J. Y.; Bromley, S. T.; Illas, F. When Anatase Nanoparticles Become Bulklike: Properties of Realistic TiO_2 Nanoparticles in the 1–6 nm Size Range from All Electron Relativistic Density Functional Theory Based Calculations. *J. Chem. Theory Comput.* **2017**, *13*, 1785-1793.

(62) Blum, V.; Gehrke, R.; Hanke, F.; Havu, P.; Ren, X.; Reuter, K.; Scheffler, M.; Havu, V. Ab Initio Molecular Simulations with Numeric Atom-Centered Orbitals. *Comput. Phys. Commun.* **2009**, *180*, 2175-2196.

(63) Muscat, J.; Wander, A.; Harrison, N. M. On the Prediction of Band Gaps from Hybrid Functional Theory, *Chem. Phys. Lett.* **2001**, *342*, 397-401.

(64) Moreira, I. de P. R.; Illas, F.; Martin, R. L. Effect of Fock Exchange on the Electronic Structure and Magnetic Coupling in NiO. *Phys. Rev. B* **2002**, *65*, 155102.

(65) Isseroff, L. Y.; Carter, E. A. Importance of Reference Hamiltonians Containing Exact Exchange for Accurate One-Shot *GW* calculations of Cu_2O. *Phys. Rev. B* **2012**, *85*, 235142.

(66) Liao, P.; Carter, E. A. Testing Variations of the *GW* Approximation on Strongly Correlated Transition Metal Oxides: Hematite (α-Fe_2O_3) as a Benchmark. *Phys. Chem. Chem. Phys.* **2011**, *13*, 15189-15199.

TOC